DOI: 10.1002/fuce.202000061

Fe_3O_4@SiO_2@CuZnAl-O Catalysts for Conversion of Lignin in Supercritical Methanol▲

J. Chen[1,2], S. Hui[1,2], G. Bao[1,2]*, J. Luo[3], Y. Meng[1,2], J. Li[1,2], A. Wang[1,2], S. Liang[1,2]

[1] State Key Laboratory of Complex Nonferrous Metal Resources Clean Utilization Kunming University of Science and Technology, Kunming 650093, China
[2] Faculty of Metallurgy and Energy Engineering, Kunming University of Science and Technology, Kunming 650093, China
[3] Biomass Group, Key Laboratory of Tropical Plant Resources and Sustainable Use, Xishuangbanna Tropical Botanical Garden, Chinese Academy of Sciences, Kunming 650223, China

Received March 31, 2020; accepted October 18, 2020; published online February 9, 2021

Abstract

The catalytic degradation of lignin was exploited by magnetic core-shell Fe_3O_4@SiO_2@CuZnAl-O catalysts in supercritical methanol (sc-MeOH) over temperature from 260 °C to 360 °C and the reaction time ranging from 0.5 h to 5 h. The magnetic core-shell-structured Fe_3O_4@SiO_2@CuZnAl-O catalysts with different mole ratio of Cu to Zn were prepared by parallel flow co-precipitating method. Catalyst Fe_3O_4@SiO_2@$Cu_{1.2}Zn_{4.8}Al_2$-O with the maximum specific surface area (142.8 $m^2 g^{-1}$) exhibited the highest lignin conversion of 66% and high selectivity for phenols, ketones and benzenes. The recyclable Fe_3O_4@SiO_2@CuZnAl-O catalyst allows high catalytic activity and selectivity for phenols, ketones and benzenes in the catalytic conversion of lignin in supercritical methanol. It is believed that this study can provide a promising strategy to prepare core–shell structured base metal nanocatalysts with metal-oxide shells.

Keywords: Alkali Lignin, Catalytic Conversion, Core-shell Structure, CuZnAl Catalyst, Supercritical Methanol

1 Introduction

The researches of the conversion of lignocellulosic biomass have attracted extensive attention considering the energy crisis and pollution problems caused by burning fossil fuel. It is well known that lignin is one ingredient of lignocellulosic biomass that provide regenerated aromatic groups [1, 2]. Therefore, the conversion of lignin into high-quality liquid fuel and valuable chemicals is of great significance to promote the development of biomass energy technology [3].

Biomass catalytic conversion in solvent is one of the main ways to use biomass resources efficiently [4, 5], and the solvent exerts a significant effect [6]. Supercritical methanol (>240 °C, >8.09 MPa) is one of the most widely used solvents because the lower dielectric constant enables dissolution of macromolecular substances easily produced by biomass degradation [7–9].

Copper-based catalysts have been widely used in the liquefaction process of lignin due to their weak acidity, high hydrogenolysis and hydrogenation effect [10–15]. Copper-based catalysts were studied for deoxidation and hydroliquefaction of a variety of lignin model compounds [10]. The addition of Zn into conventional catalyst would improve the activity of the catalyst through changing the surface structure of the catalyst and forming a porous structure [16]. The effect of ratio of Cu/Zn on converting furfural to 2-methyl furan was studied and the yield of 2-methyl furan reaches 72% when Cu/Zn is 2.5 [17]. However, the recyclability and selectivity are the main issues seriously restricting the catalytic performances in the practical applications. The preparation of magnetic core-shell catalysts was a promising way to solve the problem. Magnetic

---

▲ *Paper presented at the 2019 International Conference on Power Engineering (ICOPE2019), 21–25 October 2019, Kunming, Yunnan Province, People's Republic of China.*

[*] *Corresponding author, baoguirong@kust.edu.cn*

hydrotalcite-like Fe_3O_4@CuMgAl-LDH (LDH-Layered Double Hydroxide) catalyst was studied for the hydroxylation of phenol and 47.2% of the phenol was converted [18]. The cheap and non-toxic copper-zinc-aluminum catalyst was also applied in preparation of methanol [16], furfuryl alcohol [19], syngas [20], however, there are few reports on the catalytic conversion of lignin with the magnetic core-shell copper-zinc-aluminum catalysts.

In this paper, the magnetic core-shell complex oxide Fe_3O_4@SiO_2@CuZnAl-O catalysts were synthesized by co-precipitation method [21], and the layer of SiO_2 isolated the catalyst shell from the magnetic core to prevent their reaction during the calcination process. The effect of Cu^{2+}/Zn^{2+} molar ratio, reaction temperatures and reaction time on the conversion of lignin was studied. The catalysts were characterized by XRD, SEM, TEM, N_2 adsorption/desorption and VSM (vibrating sample magnetometer), and the liquid products were detected by GC-MS.

2 Experimental

2.1 Materials and Chemicals

$Cu(NO_3)_2·3H_2O$, NaOH, and anhydrous methanol were all obtained from Tianjin Fengchuan Chemical Reagent Technology Co. $Zn(NO_3)_2·6H_2O$ was purchased from Guangdong Fine Chemicals R & D Center. $Al(NO_3)_3·9H_2O$, Na_2CO_3 and anhydrous methanol were provided by Shantou Xilong Chemical Co. Alkali lignin was obtained from Tokyo Chemical Industry Co. All reagents were analytical reagent-AR.

2.2 Catalyst Preparation

The magnetic Fe_3O_4 nanoparticles were prepared according to [22]. 4.32 g of $FeCl_3·6H_2O$ was first dissolved in 160 mL of ethylene glycol under magnetic stirring for 1 h. 0.5 g of sodium dodecyl sulfate (SDS) and 3.6 g of sodium acetate trihydrate were then added into the above mixed solution. After continuous stirring for another 1 h, the resultant solution was poured into a 200 mL of Teflon-lined autoclave and heated for 14 h at 200 °C. The Fe_3O_4 nanoparticles were collected using a magnet, washed three times with deionized water and ethanol, dried for 6 h at 60 °C in a vacuum oven and ground in an agate mortar.

The Fe_3O_4@SiO_2 nanoparticles were prepared according to [23]. 0.36 g of Fe_3O_4 nanoparticle powder, 150 mL absolute ethanol, 50 mL of ultrapure water, and 3.4 mL of ammonia water were placed in a round bottom flask and ultrasonically shook for 30 min to form a suspension. Then, 0.6 mL of tetraethyl orthosilicate (TEOS) was poured into the suspension and magnetically stirred for 4 h. The Fe_3O_4@SiO_2 nanoparticles were obtained after washing 4 times with ethanol, magnetic separation, vacuum drying for 6 h at 60 °C and grinding in an agate mortar.

The Fe_3O_4@SiO_2@CuZnAl-O catalyst precursor was prepared by a parallel flow coprecipitating method. Calculated masses of $Cu(NO_3)_2·3H_2O$, $Zn(NO_3)·6H_2O$ and $Al(NO_3)_3·9H_2O$ with $Cu^{2+}/Zn^{2+}/Al^{3+}$ molar ratios of x:(6–x):2 (x = 1,1.2,1.5, 2, 3) were dissolved in 50 mL of ethylene glycol under stirring for 1 h. 0.3 g of Fe_3O_4@SiO_2 nanoparticle powder was mixed with 50 mL of ethylene glycol under ultrasonically shaken and the resultant suspension was loaded into a 250 mL of three-necked flask. A mixed solution of Na_2CO_3-NaOH with the mass ratio of 1:5 was selected as the precipitant. The prepared nitrate glycol mixture and the precipitant were separately placed in a 125 mL separatory funnel. The three-necked flask containing the Fe_3O_4@SiO_2 suspension was heated in a water bath maintained at the temperature of 60 °C and stirred at 500 r min^{-1}. Titration was carried out with the pH of 8.5, and the mixture was kept treating for 4 h at 60 °C after the titration. The precipitate was washed six times with alcohol and water and was dried in a vacuum drying oven for 6 h at 60 °C to obtain a Fe_3O_4@SiO_2@CuZnAl-LDH catalyst precursor. The Fe_3O_4@SiO_2@CuZnAl-O was obtained by grinding the precursor, calcining in a tube furnace at 500 °C under a nitrogen atmosphere for 2 h, and cooling down to room temperature under nitrogen atmosphere.

2.3 Characterizations

The X-ray diffraction (XRD) patterns were measured on D/max-2200 (Nippon Science and Technology Co. Ltd) operating at the scanning range from 5° to 90° with scanning speed of 10° per min. The morphologies and structures of the solid catalysts were characterized by scanning electron microscopy (SEM, Shimadzu EPMA-8705) and transmission electron microscopy (TEM, FEI JEM-2100F). SEM was performed at the resolution of 2 µm and the magnification of 20,000X. TEM was performed at the resolution of 100 nm and the magnification of 40,000X. The specific surface area was determined by the N_2 adsorption/desorption experiment (NOVA 2200e automatic nitrogen adsorption specific surface tester from Conta Instruments) operating at liquid nitrogen temperature (–196 °C). The magnetic properties of the catalyst was conducted by using vibrating sample magnetometer(VSM) (Model 7410 from Lake Shore Co.).

2.4 Conversion of Lignin

Stock solutions for reactions were prepared with 60 mg of lignin and 3.0 mL of methanol. Catalytic reactions were performed in a high-pressure mini- autoclave reactor (5 mL total volume) using the general protocol described previously [24]. Typically, 30 mg of Fe_3O_4@SiO_2@CuZnAl-O catalysts and 3.0 mL of aliquot of the stock solution were added into the reactor, which was then sealed tightly. The reactor was then placed into a molten tin bath after oscillating in an ultrasonic pool for 2 min. The reactor was quenched in a water bath at room temperature after the designated reaction time from 0.5 h to 5 h and the temperature from 260 °C to 360 °C. The liquid and solid contents were separated by centrifugal equipment and sand core filter device. The solid residue was dried in an oven at 105 °C to a constant weight.

Quantitative analysis of liquid products was performed on a TRACEDSQ gas chromatography-mass spectrometer equipped with HP-5MS (30 mm 0.25 mm 0.25 μm) quartz capillary column. In detail, 1 μL of samples were injected at a temperature of 250 °C in split mode with a ratio of 30:1, pressure flow control mode at 100 kPa, and 1.4 mL min^{-1} column flow. The carrier gas is helium. The temperature program started holding at 50 or 70 °C for 2 min followed by a 5 °C min^{-1} ramp up to 250 °C. EI with an electron energy of 70 eV was set in the MS device. The corresponding MS program had an ion source temperature at 230 °C, the quadrupole temperature is 150 °C, and the mass ranges from 45 to 500. The percentage of each component in the liquid product was calculated by the area normalization method.

The conversion rates of lignin were calculated by Eq. (1) as below:

$$C = \left(1 - \frac{m_1 - m_2}{m_0}\right) \times 100\% \tag{1}$$

where C is the lignin conversion rate (%), m_0 denotes the lignin mass (mg), m_1 and m_2 are the mass of solid residue (mg) and the catalyst mass (mg), respectively.

2.5 *Pressure in the Reactor*

The pressure in the reactor was calculated by using the van der Waals equation of state for the actual gas [25], denoted as Eq. (2).

$$\left(P + n^2a/V^2\right)(V - nb) = nRT \tag{2}$$

where P is the pressure, V the volume, T the temperature, n the amount of substance (in moles), and R the gas constant. The van der Waals constants a and b are characteristic of the substance and are independent of temperature. According to [26], constant a and b of methanol is 9.476 bar L^2 mol^{-2} and 0.0659 L mol^{-1}, respectively.

Assuming that only 0.5 mL of methanol was vaporized in the reactor, the reaction temperature was 260 °C, and the container volume was 5 mL, the pressure value was calculated as 13.08 MPa. The critical temperature of methanol is 240 °C and the critical pressure of methanol is 8.09 MPa. Therefore, if more methanol is gasified and the reaction temperature is higher than 260 °C, methanol in the reactor should be in the supercritical state.

3 Results and Discussion

3.1 *Catalyst Characterization*

It can be noted in Figure 1 that the prepared Fe_3O_4@SiO_2@CuZnAl-O catalysts maintain a good microsphere structure during synthesis. The average particle size of Fe_3O_4, Fe_3O_4@SiO_2 and Fe_3O_4@SiO_2@ CuZnAl-O were determined to be 349.7, 366.7, and 377.3 nm, respectively, after measuring more than 140 particles. As implied in Figures 2a and 2b, SiO_2 (transparent layer with the thickness of 17 nm) was effectively and firmly deposited on the surface of Fe_3O_4 microspheres. The Fe_3O_4@SiO_2@CuZnAl-O catalysts with a core-shell structure was formed as shown in the TEM images.

The change in the crystalline structure of catalysts during surface modification was investigated using XRD. The characteristic peaks of the face-centered cubic lattice of Fe_3O_4 at 2θ = 18.3°, 30.1°, 35.5°, 43.1°, 53.6°, 57.1°, 62.6° are clearly observed. Theses peaks were assigned to (111), (220), (311), (400), (422), (511), (440), and (533) of Fe_3O_4 [27], respectively. No variation of diffraction peaks corresponding to Fe_3O_4 particles was observed upon coating with a layer of SiO_2 on the surface of Fe_3O_4, but the diffraction intensity was slightly weakened. No diffraction peaks of silicon were observed on the surface of the material, indicating that SiO_2 phases exist in an amorphous form [28].

Figures 3c and 3d show the XRD results of Fe_3O_4@SiO_2@ CuZnAl-LDH and Fe_3O_4@SiO_2@CuZnAl-O. It can be noted that the catalyst precursor is mainly composed of hydrotalcite-like layered double hydroxide phase of $Cu_2Zn_4Al_2(OH)_{16}CO_3{\cdot}4H_2O$. The catalyst precursor (Figure 3c) not only exhibited characteristic diffraction peaks corresponding to Fe_3O_4, but also characteristic peaks of

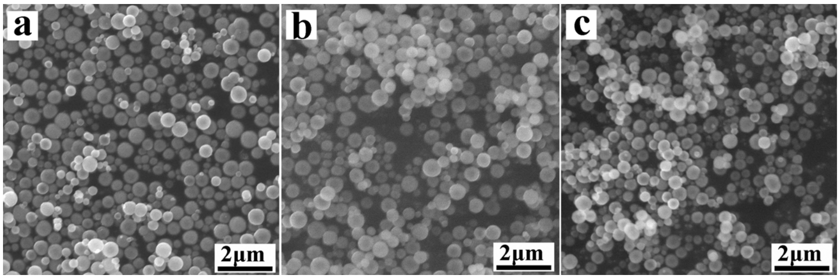

Fig. 1 SEM images of (a) Fe_3O_4, (b) Fe_3O_4@SiO_2, and (c) Fe_3O_4@SiO_2@CuZnAl-O.

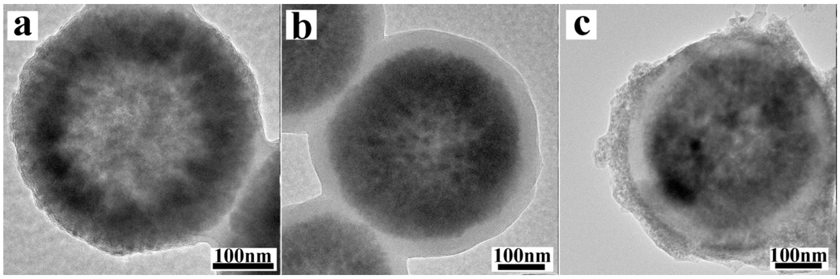

Fig. 2 TEM images of (a) Fe_3O_4, (b) Fe_3O_4@SiO_2, and (c) Fe_3O_4@SiO_2@CuZnAl-O.

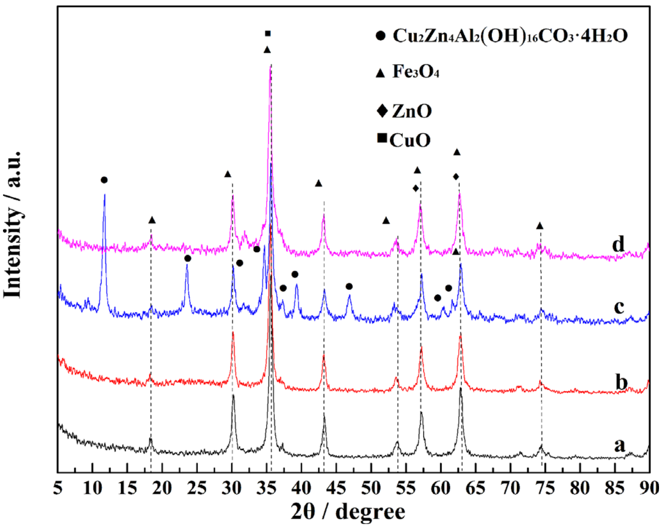

Fig. 3 XRD patterns of (a) Fe_3O_4, (b) Fe_3O_4@SiO_2, (c) Fe_3O_4@SiO_2@-CuZnAl-LDH, and (d) Fe_3O_4@SiO_2@CuZnAl-O.

CuZnAl-LDH. The characteristic diffraction peaks of CuZnAl-LDH at 11.7° disappeared due to calcination (Figure 3d). The diffraction peak at around 35.5° was assigned to the diffraction of (111) of CuO [29]. The diffraction peaks at around 56.76° and 62.7° belonging to (110) and (103) of ZnO were observed [30]. These indicated that the main components of the prepared Fe_3O_4@SiO_2@CuZnAl-O were Fe_3O_4 and copper-zinc-aluminum composite oxide.

Figure 4 shows the XRD patterns of Fe_3O_4@SiO_2@CuZnAl-O catalysts with different Cu/Zn molar ratios. Slightly changed positions and widths of the diffraction peaks with different Cu/Zn molar ratios were observed, indicating that the content of Cu has negligible effect on the crystal structure of the catalysts.

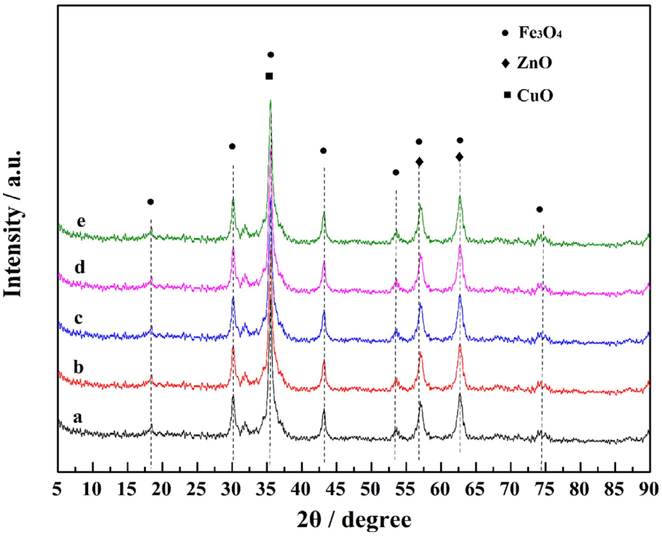

Fig. 4 XRD patterns of Fe_3O_4@SiO_2@$Cu_xZn_{6-x}Al_2$-O catalysts (x = 1, 1.2, 1.5, 2, and 3 for curves a, b, c, d, and e, respectively).

The N_2 adsorption/desorption isotherms of the samples are illustrated in Figure 5. The adsorption isotherms of all the samples belong to the IV type in the IUPAC classification, and had a type 3 hysteresis loop (H3) [31]. The specific surface areas of the catalysts Fe_3O_4@SiO_2@$Cu_xZn_{6-x}Al_2$-O (x = 1, 1.2, 1.5, 2, 3) were found to be 135.8, 142.8, 115.6, 112.3, and 104.3 $m^2 g^{-1}$, respectively. The Fe_3O_4@SiO_2@$Cu_{1.2}Zn_{4.8}Al_2$-O catalyst had the maximum specific surface area of 142.8 $m^2 g^{-1}$, indicating that too high or too low ratio of Cu will reduce the specific surface area of the catalyst. The actual molar ratios of Cu, Zn, and Al (0.173:0.682:0.272) has been determined by ICP-OES analysis from our previous work [32].

Figure 6 displays the hysteresis curves of Fe_3O_4, Fe_3O_4@SiO_2, Fe_3O_4@SiO_2@CuZnAl-LDH and Fe_3O_4@SiO_2@CuZnAl-O catalyst at room temperature, which exhibit typical S-shaped magnetization curve of superparamagnetic materials. The saturation magnetization of Fe_3O_4, Fe_3O_4@SiO_2, and Fe_3O_4@SiO_2@CuZnAl-O catalysts were 71.6 emu g^{-1}, 58.9 emu g^{-1}, and 36.1 emu g^{-1}, respectively. It could be concluded that the maximum saturation magnetization decreased after cladding became thick, and the magnetic properties did not decrease significantly after the catalysts were calcined. It has been reported that substances with saturation magnetic strength greater than 16.3 emu g^{-1} can be easily attracted to magnets [31]. The obvious separation by a magnet can be noted from the Figure 6 in the lower right corner. Therefore, the obtained Fe_3O_4@SiO_2@CuZnAl-O catalysts exhibited excellent magnetic properties and could be easily separated from the reaction liquid with a magnetic separation method.

3.2 *Conversion of Lignin*

The conversion rate of lignin was observed in Figure 7 ($Cu_xZn_{6-x}Al_2$; x = 1, 1.2, 1.5, 2, 3, labeled as M_1, $M_{1.2}$, $M_{1.5}$, M_2, M_3, respectively). The conversion rate of lignin was boosted up to 66.55% when the molar ratio of Cu: Zn is 1.2:4.8 (Fe_3O_4@SiO_2@$Cu_{1.2}Zn_{4.8}Al_2$-O) in the catalyst, indicating that the proper ratio of copper to zinc can lead to the high conversion rate of lignin. Fe_3O_4@SiO_2@$Cu_{1.2}Zn_{4.8}Al_2$-O had the largest specific surface area so that the most active sites were beneficial to methanol-reforming, promoting the lignin reaction and conversion rate. Subsequent studies on the effect of temperature and reaction time were conducted based on this catalysts.

3.2.1 *Effect of Reaction Time*

The effect of reaction time in a range of 0.5–5 h at 300 °C was investigated. As the reaction time increase, the conversion rate of lignin increase, as shown in Figure 8. The lignin conversion rate increased significantly from 0.5 h to 2.5 h, increased by 15.26% from 51.79% (0.5 h) to 67.05% (2.5 h). But from 2.5 h, the change of conversion rate is relatively smooth. This is because the ether bond breakage is basically completed after lignin is reacted for 2.5 h at 300 °C. However, the temperature

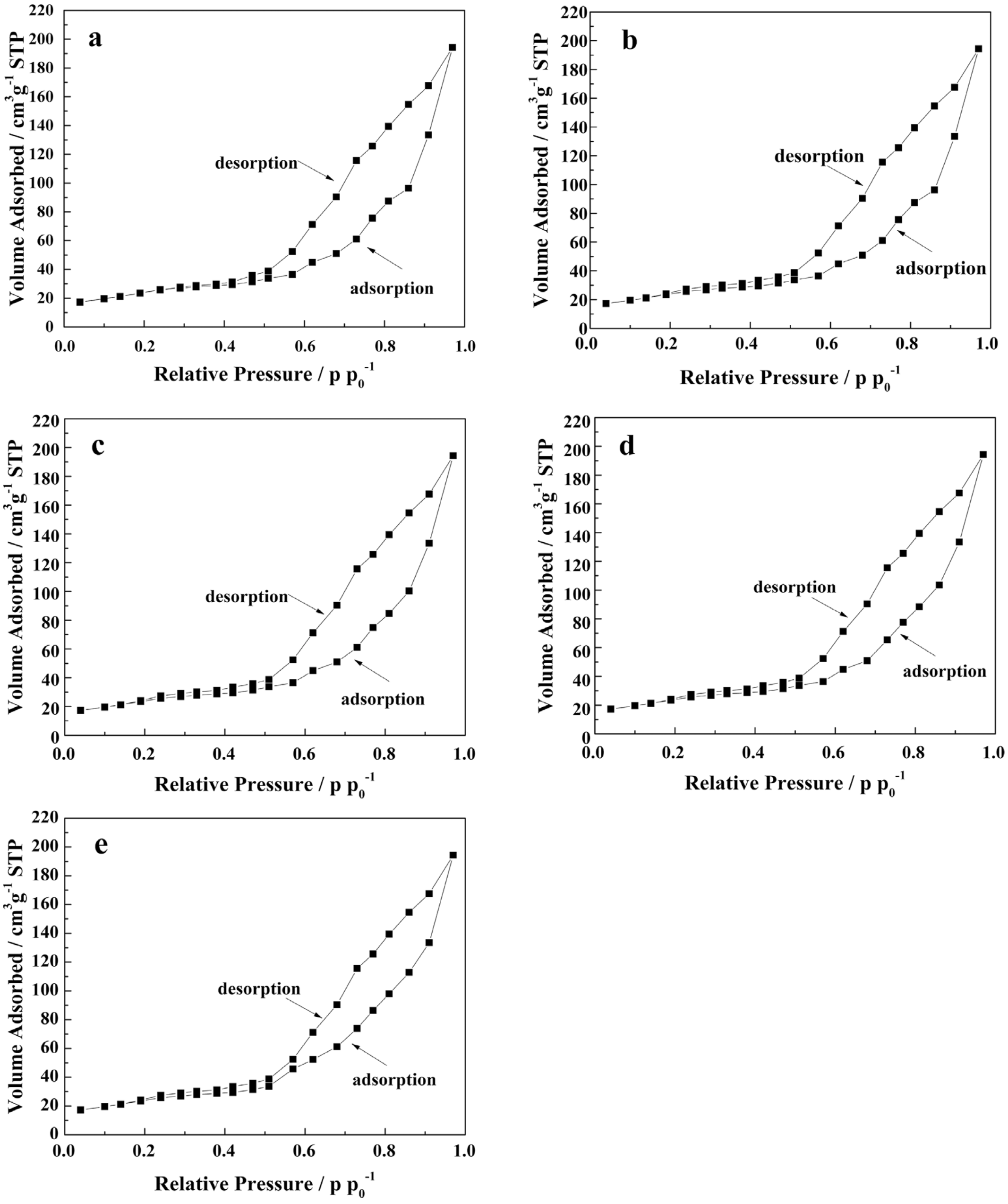

Fig. 5 N_2 adsorption-desorption isotherms of Fe_3O_4@SiO_2@$Cu_xZn_{6-x}Al_2$-O catalysts (x = 1, 1.2, 1.5, 2, and 3 for curves a, b, c, d, and e, respectively).

of 300 °C is not enough to destroy the C–C bond and C=C bond in lignin.

Figure 9 or Table 1 show that the products from catalytic liquefaction of lignin were mainly phenols, ketones, benzenes and alcohols. The products were mostly phenols, alkanes and ketones when the reaction time was short. As the reaction time was prolonged, phenols and ketones decreased, and hydrocarbons increased, this was caused by the conversion of phenols into hydrocarbons. It should be noted that the main liquefaction product was phenols (65% at 0.5 h) due to the breakage of ether bonds such as β-O-4, α-O-4, 4-O-5 and α-O-γ in basic structural units in lignin. In supercritical methanol, ether bonds of lignin can be cracked and decomposed into some monomer compounds including phenols and other types of products. Ketones are formed through condensation reaction of phenolic monomers as the reaction time increases [33]. But the formation path of ketone products is not clear and needs further research and confirmation. On the other hand, oxygen atoms can be selectively removed from phenols through hydrodeoxygenation (HDO), dehydration, decarboxylation, etc. to form benzenes [34]. At shorter reaction time, less hydrogen is generated because of the low rate of methanol reformation, which affects the hydrogenolysis of lignin, resulting in fewer products. It can be observed from Table 1 that only

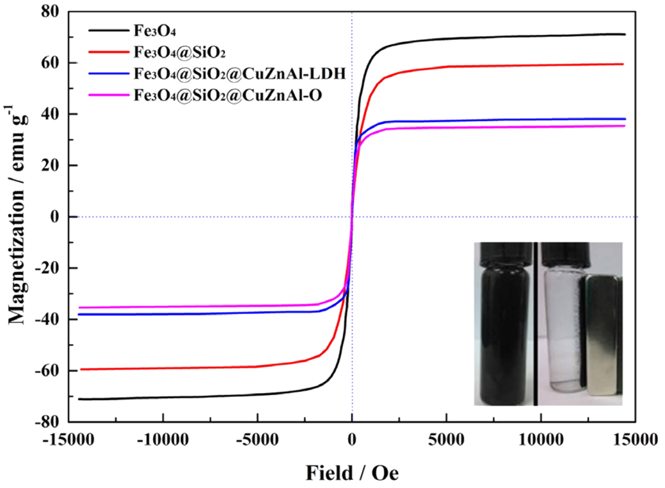

Fig. 6 Magnetic hysteresis curves of Fe_3O_4, $Fe_3O_4@SiO_2$, $Fe_3O_4@SiO_2@CuZnAl\text{-}LDH$, and $Fe_3O_4@SiO_2@CuZnAl\text{-}O$.

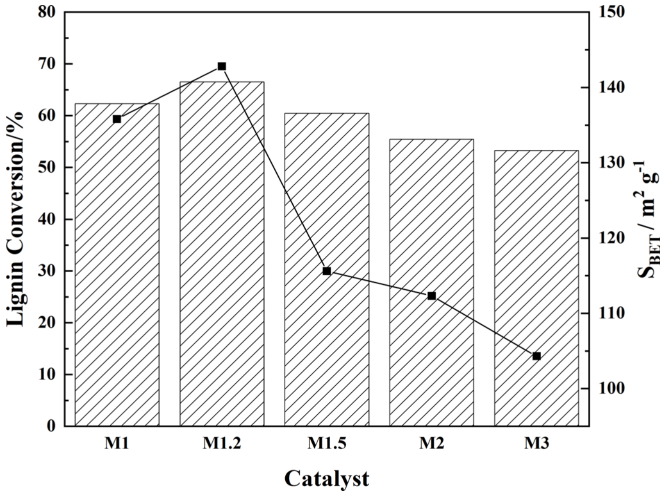

Fig. 7 The variation of specific surface area of solid catalysts and lignin conversion rate with the molar ratio of Cu to Zn.

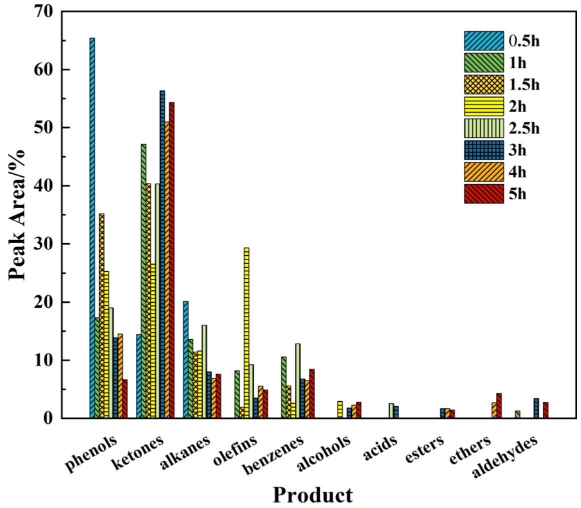

Fig. 9 Products from lignin catalytic liquefaction at different times.

8 kinds of products were obtained in half an hour. The type of product remains basically unchanged ranging from 1 to 4 h, but further increases to 21 by 5 h. It shows that the generated small molecular substances reacted further, producing more by-products after a long time of reaction [35].

3.2.2 Effect of Reaction Temperature

The effect of reaction temperature in a range of 260 – 360 °C was investigated at the reaction time of 1 h. With the increase of temperature, lignin conversion rate increased from 45.52% at 260 °C to 78.55% at 360 °C, as shown in Figure 10. During the conversion of lignin from 260 °C to 320 °C, the C–O bond and ether bond were mainly broken. When the temperature is higher than 320 °C, the main reason for the conversion of lignin is the breakage of the C–C bond, and C=C bond and the hydrogenation of the aromatic ring. Therefore, higher temperature is conducive to the liquefaction of lignin. The main products were compared in Figure 11 or Table 2 The results show

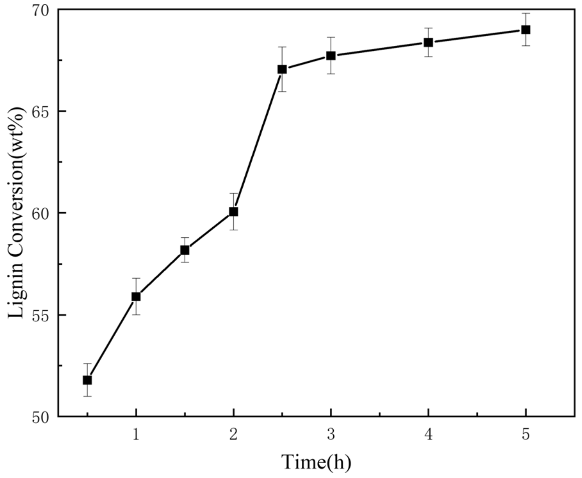

Fig. 8 Lignin conversion rates at different times.

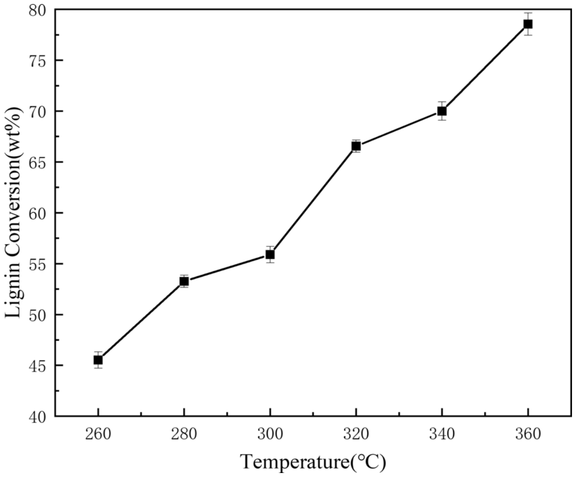

Fig. 10 Lignin conversion rates at different temperatures.

Table 1 The main products of lignin liquefaction at different time.

Products	Area (%)								Qual
	0.5h	1h	1.5h	2h	2.5h	3h	4h	5h	
2,2-dimethoxybutane	3.942	1.8959	–	2.3245	2.385	1.8254	–	1.5973	83
2-methoxyphenol	22.798	1.864	4.138	–	–	–	–	–	97
2-methoxy-4-methylphenol	7.4683	9.6935	–	7.0874	4.1616	–	–	–	86
2-methoxy-4-methylphenol	21.188	–	–	–	–	–	–	–	96
4-isopropylthiophenol	13.964	–	–	–	–	–	–	–	80
2,5-dimethyl-4-hydroxy-3-hexanone	10.99	2.3594	4.888	6.4332	4.2701	2.6582	–	1.4776	78
Undecane	16.235	11.698	6.3011	9.2861	9.8513	6.1867	6.8614	6.0006	91
2,5-dihydroxyacetophenone	–	15.501	31.609	27.301	28.141	30.02	33.881	28.082	86
3,4,4-trimethyl 2-cyclopentene	–	8.1989	–	–	–	–	–	–	83
1,2-dimethoxybenzene	–	8.3783	2.7116	2.6427	3.7185	–	2.7871	–	91
2-methoxy-6-methylphenol	–	1.8291	12.731	10.086	8.2406	5.8617	7.9389	–	87
2-hydroxy-4-acetophenone	–	22.208	–	–	–	–	–	–	87
2-methoxy-4-propyl-phenol	–	3.9125	–	–	–	–	–	–	72
1,2,-dimethoxy-4-propylbenzene	–	2.2004	–	–	–	–	–	–	64
2-methoxy-4 methylphenol	–	–	10.156	–	–	–	–	–	91
P-tert-butylcatechol	–	–	8.1549	–	6.6035	8.0241	–	–	86
3,4-dimethoxytoluene	–	–	2.8628	–	4.4274	–	–	–	56
Methyl 2-methylbutyrate	–	–	–	–	–	1.6812	1.6639	1.4394	74
2-methyl-1-cyclopentene ethyl ketone	–	–	–	2.1683	–	–	–	–	78
4-methoxy-2,3,6-trimethylphenol	–	–	–	8.159	–	–	6.5954	–	86
2,4-dihydroxy-3-methoxyacetophenone	–	–	–	3.9157	–	4.1687	–	–	59
2,4-dimethyl-3-pentanone	–	–	3.8568	5.7086	7.9244	5.6427	4.7755	5.651	83
1,2-methoxy-4-propylbenzene	–	–	–	–	4.6755	–	–	4.4701	83
1,3-dimethoxybenzene	–	–	–	–	–	2.6096	–	–	59
3,4-dimethoxyacetophenone	–	–	–	–	–	3.4851	–	–	72
4-methylthio-phenylethanone	–	–	–	–	–	5.3005	4.3801	–	87
2,6-dimethylcyclohexanone	–	–	–	–	–	5.0702	4.6092	–	72
Trans-2,2-dimethyl-3-heptene	–	–	–	–	3.8166	–	–	2.9907	64
2,3,4-trimethylcyclopentene	–	–	–	–	–	–	–	1.8892	90
1,2,-dimethoxybenzene	–	–	–	–	–	–	–	1.8804	91
2-methoxy-3-methylphenol	–	–	–	–	–	–	–	6.6645	91
2,3-dimethoxytoluene	–	–	–	–	–	4.174	3.7094	2.0899	93
4-acetoxy-3-p-methoxyacetophenone	–	–	–	–	–	–	–	4.6612	83
2-hydroxy-6-methoxyacetophenone	–	–	–	–	–	–	–	8.8551	86
4-hydroxy-3-tert-butyl-anisole	–	–	–	–	–	–	2.7207	4.2807	72

that the reaction products became more complex as the temperature increases.

The products were mainly phenols, alkanes, and ketones below 300 °C. The main product was phenols at 260 °C and 280 °C (over 50%), because the ether bonds in lignin could be easily broken at low temperatures phenols, the production of alkanes decrease with the increase of temperature. But ketones reach the highest concentration of 47.13% at higher temperature of 300 °C. Small amount of olefins, benzenes, alcohols, esters and aldehydes were formed at high temperatures due to the condensation and recombination reactions.

It can be observed from Table 2 that the types of reaction products increase from 6 to 27 as the temperature increases. Lignin conversion in supercritical methanol is dominated by catalytic hydrogenolysis. The methanol-reforming rate is slow at low temperatures (less than 300 °C), resulting in lower hydrogenolysis rate of lignin. Therefore, fewer products are released in this temperature range. The depolymerization

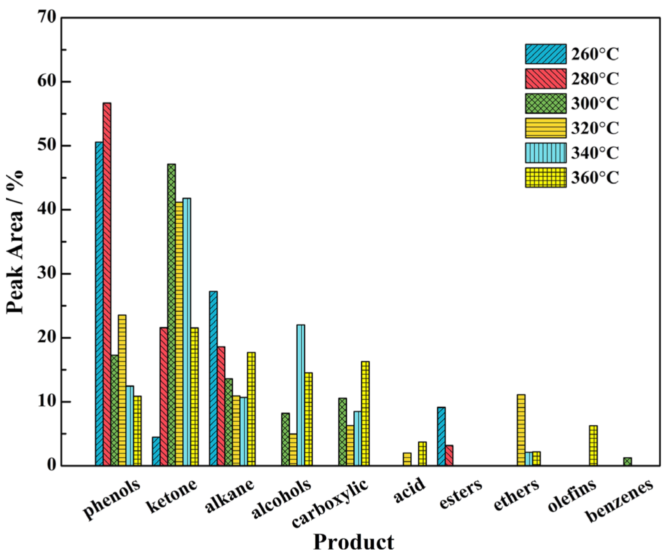

Fig. 11 Products from lignin catalytic liquefaction at different temperatures.

reaction is enhanced as the temperature rises, so more stubborn lignin structures can be cracked, producing more lignin fragments [36].

4 Conclusion

In summary, magnetic Fe_3O_4@SiO_2@CuZnAl-O catalysts with a core-shell structure were successfully synthesized by coating Fe_3O_4 microspheres with SiO_2 and CuZnAl-O shells. The catalyst had a saturation magnetization of 36.1 emu g^{-1} with a strong magnetic response capability. The ratio of Cu/Zn influenced the specific surface area of the catalysts and the conversion rate of lignin. Fe_3O_4@SiO_2@$Cu_{1.2}Zn_{4.8}Al_2$-O with maximal specific surface area subsequently provided the highest lignin conversion rate. The lignin liquefaction products were mainly composed of phenols, ketones and alkanes. Phenols could be formed at low temperature and short reaction time and ketones could be obtained at high temperature and long reaction time through the cleavage of ether bonds.

Table 2 The main products of lignin liquefaction at different temperatures.

Products	Area (%)						Qual
	260 °C	280 °C	300 °C	320 °C	340 °C	360 °C	
Propionic acid	9.1301	3.159	–	–	–	–	64
2-methyl-3-pentanone	–	2.5901	2.1817	–	–	–	90
2,2-dimethoxybutane	5.4679	3.0716	1.8959	1.7498	2.2118	1.2535	83
2-methoxyphenol	30.9267	18.2975	1.864	4.8339	–	–	83
2-methoxy-4-methylphenol	19.6433	–	9.6935	5.454	–	–	91
1,2-dimethoxybenzene	–	–	8.3783	3.0883	3.5079	3.9152	94
2-methoxy-6-methylphenol	–	–	1.8291	10.3493	8.6098	–	87
2-methoxy-4-propyl-phenol	–	3.4125	3.9125	–	–	–	90
1,2,-dimethoxy-4-propylbenzene	–	–	2.2004	–	–	–	64
1,2,3-trimethylcyclohexane	–	2.4598	–	1.8716	–	2.7298	53
Methyl 2-methylbutyrate	–	–	–	–	2.1252	2.1937	83
4-methoxy-2,3,6-trimethylphenol	–	–	–	–	–	2.0943	86
2,4-dimethyl-3-pentanone	–	–	–	3.8364	4.6676	3.6553	90
2,4-dimethyl-3-pentanol	–	–	–	–	–	3.7148	64
Trans-5-decene	–	–	–	2.3342	2.7427	–	64
2-hydroxy-4 acetophenone	–	–	22.2081	–	–	–	87
2,4,4-Trimethylcyclopentanone	–	–	2.657	–	–	–	64
3,4,4-trimethyl 2-cyclopentene	–	–	8.1989	–	–	–	83
Trans-2,2-dimethyl-3-heptene	–	–	–	2.6319	–	–	60
2,5-dimethyl-4-hydroxy-3-hexanone	4.4736	18.9804	2.3594	2.6646	–	–	83
Undecane	21.7947	13.0622	11.6983	7.2843	8.4829	4.7681	94
2-methoxy-5-methylphenol	–	18.7486	–	–	–	–	97
2-methoxy-4 ethylphenol	–	12.4445	–	–	–	–	91
2-methoxy-4-propyl-phenol	–	3.4125	3.9125	–	–	–	90
2-methoxy-3-methylphenol	–	3.7737	–	–	–	–	91
3-methoxy-2,4,6-trimethylphenol	–	–	–	2.904	–	–	87

Table 2. Continued.

Products	Area (%)						Qual
	260 °C	280 °C	300 °C	320 °C	340 °C	360 °C	
2-hydroxy-4-methoxyacetophenone	–	–	–	6.688	–	–	80
Methyl hexadecanoate	–	–	–	7.4965	–	–	98
16-Methylhexadecanoic acid methyl ester	–	–	–	3.6226	–	–	93
2,3-dimethyl-3-heptene	–	–	–	–	5.1278	–	60
2,3,4,5-tetramethyl-2-cyclopentene	–	–	–	–	3.9611	–	72
3,5-dimethoxytoluene	–	–	–	–	4.9631	–	93
3-hydroxy-4-methoxyacetophenone	–	–	–	–	5.3445	–	80
2,3-dimethoxytoluene	–	–	–	–	–	5.3516	93
2,3-dimethoxytoluene	–	–	–	3.206	–	2.6923	94
2,5-dihydroxyacetophenone	–	–	15.5008	24.6227	26.4207	–	86
2-hydroxy-6-methoxyacetophenone	–	–	–	–	5.3571	3.067	72
1,1,2-trimethyl-3-cyclopropane	–	–	–	–	–	3.7516	64
4-methoxy-3-methylphenol	–	–	–	–	–	1.0778	90
5-methoxy-2,3,4-trimethylphenol	–	–	–	–	–	4.258	64
4-hydroxy-2,4,5-trimethyl-2,5-cyclohexadiene	–	–	–	–	–	7.52	87
4-methylthiophenylethanone	–	–	–	–	–	8.9237	72
2,3,4,6-tetramethylphenol	–	–	–	–	–	1.6567	87
2,3,4,6-tetramethylphenol	–	–	–	–	–	2.855	87
1,4-diaminobenzene	–	–	–	–	–	3.2365	80
4-hydroxy-3-tert-butyl-anisole	–	–	–	–	–	6.2829	83

The special catalyst structure endowed the catalyst with magnetic recyclability, high catalytic activity and selectivity for phenols, ketones and alkanes.

Acknowledgements

This work was supported by the National Natural Science Foundation of China (51966008 and 51266003).

References

[1] D. G. Mulat, S. G. Huerta, D. Kalyani, *Biotechnol. Biofuels* **2018**, *11*, 19.
[2] S. Tosoni, H. T. Chen, P. A. Ruiz, *Philos. Trans. R. Soc., A* **2018**, *376*, 20170056.
[3] Y. I. Zhang, Z. Z. Wei, *Huagong Xinxing Cailiao.* **2012**, *40*, 132.
[4] M. C. Wang, *J. Polym. Sci., Part B: Polym. Phys.* **2011**, *12*, 1433.
[5] D. M. Alonso, J. Q. Bond, J. A. Dumesic, *Green Chem.* **2010**, *12*, 1493.
[6] L. Liang, J. P. Yan, Q. He, T. Luong, T. R. Pray, A. Blake, *Green Energy & Environment* **2019**, *4*, 432.
[7] M. Barati, G. K. Baseri, *Environ. Prog. Sustainable Energy* **2018**, *37*, 861.
[8] A. Toledano, L. Serrano, J. Labidi, *Fuel* **2014**, *116*, 617.
[9] G. Liu, G. R. Bao, H. Wang, J. Luo, S. Hui, Y. Huang, Y. W. Ma, *Cellulose* **2019**, *26*, 8291.
[10] J. L. Zhang, B. C. Li, W. L. Zhang, H. N. Deng, H. H. Wang, *J. Dispersion Sci. Technol.* **2020**, *41*, 3.
[11] K. L. Deutsch, B. H. Shanks, *Appl. Catal., A* **2012**, *447*, 144.
[12] S. Bhargava, H. Jani, J. Tardio, *Ind. Eng. Chem. Res.* **2007**, *46*, 8652.
[13] Z. Xia, H. Lu, H. Liu, *Catal. Commun.* **2017**, *90*, 39.
[14] Y. Zhao, S. Li, Y. Wang, *Chem. Eng. J.* **2017**, *313*, 759.
[15] J. Dantas, E. Leal, A. B. Mapossa, *Fuel* **2017**, *191*, 463.
[16] M. Behrens, F. Studt, I. Kasatkin, *Science* **2012**, *336*, 893.
[17] H. Niu, J. Luo, C. Li, *Ind. Eng. Chem. Res.* **2019**, *16*, 6298.
[18] H. Zhang, G. Zhang, *J. Mater. Chem. A.* **2013**, *1*, 5934.
[19] Y. H. Huang, G. Q. Ren, J. Sun, *Ranliao Huaxue Xuebao* **2016**, *44*, 6.
[20] X. Deng, Y. J. Liu, W. Huang, *J. Energy Chem.* **2018**, *27*, 319.
[21] T. Sugimoto, *Adv. Colloid Interface Sci.* **1987**, *28*, 65.
[22] H. W. Jing, X. M. Wang, Y. Liu, A. Q. Wang, *Chin. J. Catal.* **2015**, *36*, 244.
[23] M. P. Mazhari, M. Hamadanian, *J. Electron. Mater.* **2018**, *47*, 7484.
[24] F. G. Tan, G. R. Bao, F. S. Li, P. P. Mao, *Kunming Ligong Daxue Xuebao* **2016**, *041*, 20.

[25] D. R. Lide,, *CRC Handbook of Chemistry and Physics*, 85th Ed., National Institute of Standards and Technology, CRC press, LLC, Boca Raton, USA, **2004**.

[26] R. C. Reid, J. M. Prausnitz, B. E. Poling, *The Properties of Gases and Liquids*, 4th Ed., McGraw-Hill Book Company, New York, USA, **1987**.

[27] C. Gunathilake, J. Górka, S. Dai, M. Jaroniec, *J. Mater. Chem. A* **2015**, *3*, 30.

[28] W. J. Wang, H. P. Zhang, *Wuji Huaxue Xuebao.* **2014**, *30*, 2726.

[29] Z. Fan, L. Yuan, X. Xiao, *Fuel Process. Technol.* **2018**, *178*, 148.

[30] M. R. Nabid, R. Sedghi, S. Gholami, *Photochem. Photobiol.* **2013**, *89*, 24.

[31] S. Zhang, X. Zhao, H. Niu, *J. Hazard. Mater.* **2009**, *167*, 560.

[32] G. Liu, G. R. Bao, H. Wang, L. Jia, *Cellulose* **2019**, *26*, 8291.

[33] E. Minami, H. Kawamoto, S. Saka, *J. Wood Sci.* **2003**, *49*, 158.

[34] L. Serrano, J. A. Cecilia, G. S. Cristina, *Top. Curr. Chem.* **2019**, *377*, 28.

[35] C. M. Bernt, H. Manesewan, M. Chui, *ACS Sustain. Chem. Eng.* **2018**, *6*, 2510.

[36] X. Huang, C. Atay, J. Zhu, *ACS Sustain. Chem. Eng.* **2017**, *5*, 10864.